Technical Report / Research

Evaluation of Fatigue Property of Full-scale Axles for Railway Vehicles and Its Application to Fatigue Damage Evaluation Standard

Taizo MAKINO*
Chihiro KOZUKA
Miyuki YAMAMOTO
Hiroki SAKAI
Yosuke YAMAZAKI
Kohji MINOSHIMA

Abstract

Fatigue-limit-based designs were employed for railway axles in Japan, and new strength design and evaluation standards were developed to achieve more practical designs. The design standard for strength was introduced to describe the detailed processes, whereas the evaluation standard for damage was introduced to propose a method for the estimation of the fatigue damage caused by variations in in-service conditions. Further, safety assessments were implemented by comparing the equivalent stress with the reference values obtained from past safe-operation records. In the proposed method, slopes of S–N curves are crucial for the calculation of the equivalent stress. Thus, full-scale fatigue tests were performed on quenched and tempered and induction hardened axles used in Japan and S–N curves of fitted and non-fitted parts were examined.

1. Introduction

Railway axles are used in a configuration called a wheelset. The wheelset has two wheels fitted (press-fitted) to both sides of the axle. As shown in **Fig. 1**, the wheelset rotates while being subjected to vertical force caused by the weight and vibration of the vehicle, horizontal centrifugal force when passing through curves, and reaction force from the rails. The axle is thus subjected to rotating bending under actual operation.[1, 2] For this reason, strength design against fatigue damage is essential.

In Japan, axles have been designed based on fatigue limits for many years. However, to achieve a more rational design, new strength design and damage assessment methods were considered. The Japan Association of Rolling Stock Industries (JARi) established the following standards in September 2016.

JRIS D1201-1 Rolling stock - Axle strength - Part 1: Design method[3]
JRIS D1201-2 Rolling stock - Axle strength - Part 2: Fatigue damage evaluation method[4]

In the strength design method of JRIS D1201-1, the maximum stress that can occur in axles, depending on the track conditions and design speed, is estimated. The shape of the axles is designed to ensure a certain safety factor against the fatigue limit. This method is similar to the conventional design method in Japan. However, in JRIS D1201-1, the equations for calculating the loads associated

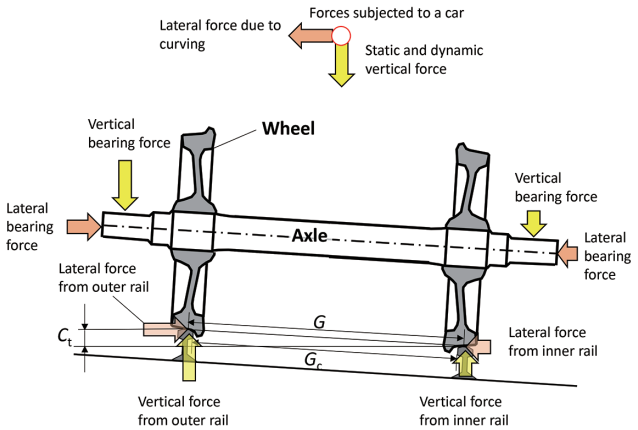

Fig. 1 Schematic illustration of configuration of wheelset and forces acting on it

* Dr. Eng., Leading Researcher, Steel Research Laboratories
1-8 Fuso-cho, Amagasaki City, Hyogo Pref. 660-0891

with driving and braking were revised compared to the conventional design method. The applicable range of vehicle speed was expanded to a higher speed range. The design procedure was specified in detail. Therefore, there are no safety concerns if the design method of JRIS D1201-1 is used. However, because the amplitude and frequency of the in-service stress change depending on the operating conditions, the accumulated fatigue damage is expected to vary despite the same safety factor.

In Europe, the members of the Technical Committee 24 of the European Structural Integrity Society (ESIS TC24) launched and promoted a joint project and achieved remarkable results with the fatigue damage evaluation of axles.[5–12] Zerbst et al.[5] clarified the effects of various parameters on the remaining life, which is the basis for setting the inspection interval from the viewpoint of the damage tolerance of axles. These parameters include material properties such as the variation of fatigue crack growth rate against the stress intensity factor range, threshold stress intensity factor range, and fracture toughness, as well as parameters that affect the load on the axle, such as fit, rotating bending, loading history, and mixed mode. Beretta et al.[6] applied a probabilistic approach to the calculation of damage values for fatigue failure and proposed a method to obtain the safety factor corresponding to the set mileage and failure probability based on the Monte Carlo simulation by taking into account the maximum allowable stress and a coefficient of variation. Traupe et al.[7] proposed a realistic method for setting the non-destructive testing (NDT) interval based on fracture mechanics calculations and crack growth tests on actual axles.

In China, Wu et al. proposed a stepwise fatigue assessment method that includes safe life in the first stage and damage tolerance in the second stage.[13–16] In the safe life stage, the damage value was evaluated using a bilinear *S–N* curve based on the FKM Guideline.[17] Based on the results, the mileage at which the damage value reached a critical value was predicted as the life.

On the other hand, we conducted fatigue tests on press-fitted axles under variable loads and considered the applicability of the linear damage law to life expectancy prediction.[18, 19] Our study found that the critical damage value changed depending on the variable load conditions and axle dimensions. This finding suggests that absolute evaluation based on a certain critical damage value is not realistic. Therefore, the applicability of relative evaluation was explored, and the damage evaluation method in JRIS D1201-2 was introduced based on this study. This method evaluates safety by estimating fatigue damage under in-service conditions and comparing the estimated fatigue damage with that of a reference axle. Since this method evaluates the safety of axles by a relative comparison of equivalent stress with axles that have performed satisfactorily, it is superior in terms of safety risk reduction compared to prior studies on axles in Europe and China.

In this report, we describe the outline of JRIS D1201-2 and present the *S–N* curves of the axles used in our evaluation, which were examined during the standardization process. Most of the contents of this report are quoted and reproduced from our reference 20) with the permission of the copyright holder.

2. Overview of Fatigue Damage Evaluation Method Standard (JRIS D1201-2)

2.1 Basic framework of damage assessment method

The standard JRIS D1201-2 is expected to help modify the axel shapes designed based on the standard JRIS D1201-1, evaluate axel redesigns in response to changes in in-service conditions, and establish more rational design methods in the future. **Figure 2** shows the flow of the fatigue damage assessment method for railway axels. First, the in-service stress spectrum is estimated. Next, the stress spectrum is compared with the stress and number of cycles to failure (*S–N*) curve to calculate the equivalent stress based on the modified Miner's rule. At this time, the *S–N* curve is expressed by:

$$N = A^* \cdot \sigma^{-m} \quad (1)$$

where N is the number of cycles to failure, A^* is the coefficient of the *S–N* curve, σ is the stress amplitude [MPa], and m is the exponent of the *S–N* curve. The damage value D_M according to the modified Miner's rule is expressed by:

$$D_M = \sum_{i=1}^{n} \frac{n_i}{N_i} \quad (2)$$

where n_i is the number of cycles of the i-th stress and N_i is the life for the i-th stress calculated from Eq. (1). As shown in the upper right corner of Fig. 2, the D_M mentioned above can also be calculated using the same Eqs. (1) and (2) at stress levels lower than the fatigue limit.

The equivalent stress σ_{eq} is defined as the stress of a constant amplitude that gives the same damage value when the total number of cycles under variable stress amplitude conditions is the same and is expressed by:

$$\sigma_{eq} = \sqrt[m]{\frac{\sum_i \sigma_i^m \times n_i}{\sum_i n_i}} \quad (3)$$

where σ_i is the amplitude of the i-th stress level.

For axles that have been proven to be fully safe in the past, their equivalent stress is calculated beforehand using the same method described above. This equivalent stress is called the reference equivalent stress.

Finally, safety is evaluated by comparing the equivalent stress and the reference equivalent stress using the equivalent stress ratio

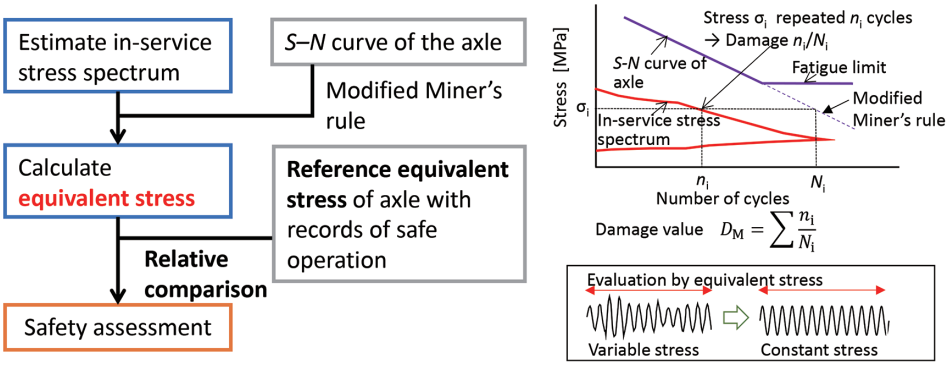

Fig. 2 Flow diagram of the evaluation method for the fatigue damage of railway axles[20]

R_S in the following equation:

$$R_S = \frac{\sigma_{eq,R}}{\sigma^*_{eq}} \quad (4)$$

where $\sigma_{eq,R}$ is the reference equivalent stress and σ_{eq}^* is the equivalent stress acting on the axle to be evaluated for fatigue damage. When R_S is 1.0 or more, the axle is judged to have a sufficient safety margin. When R_S is less than 1.0, but the axle satisfies the requirements of the strength design method in JRIS D1201-1, the axle can be used but requires careful operation.

2.2 Characteristics of damage assessment method

(1) The equivalent stress based on the modified Miner's rule is used as the damage assessment index. The slope of the *S*–*N* curve is essential for calculating the equivalent stress and was determined based on the fatigue test results.
(2) The reference equivalent stress used in the safety assessment was set based on the past safe operating record.
(3) The stress acting on the axles of newly constructed tracks or newly designed rolling stock is not measured at the design stage. For this reason, the procedure for estimating the in-service stress spectrum was formulated. It was preconfirmed that the obtained stress spectrum had high estimation accuracy.

2.3 Methods for estimating stress spectrum and equivalent stress

In this section, we introduce the methods for estimating the stress spectrum and equivalent stress defined in JRIS D1201-2. **Figure 3** shows the basic flow. Although the methods for estimating the stress spectrum have already been proposed by Braghimin et al.[21] and Watson et al.,[22] we have established our method. First, the entire railway line to be evaluated is divided into multiple evaluation segments, and the segments are classified into straight and curved elements. Then, the operating conditions of the elements (number of in-service trains, loading rate, operating speed at each point, etc.) are verified. Suppose the measurement data from real cars (referred to as "base data" from now on) are available and can be used as they are. In that case, they are directly processed as to their frequency, and the frequency distribution is prepared. If the base data cannot be used as they are because the operating conditions are different, the stress in each line segment is assumed to follow a normal distribution. The average stress σ_{av} and standard deviation σ_{dv} are determined from the curve radius and passing speed. Regarding the calculation of the average stress σ_{av}, the following Eq. (5) was derived

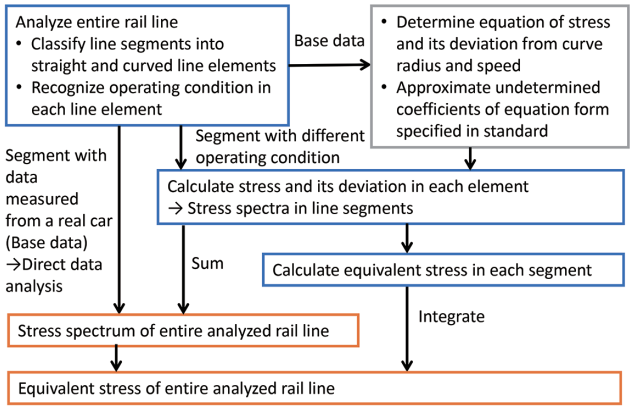

Fig. 3 Estimation of in-service stress spectrum and equivalent stress of railway axle[20]

based on the result that the relationship between the average stress σ_{av} and the curve radius R when the train passes a curve was found by a multibody simulation[23] to follow the Gompertz growth curve.[24] Concerning the calculation of σ_{dv}, the analysis of the measured data confirmed that σ_{dv} correlated with R, and the following Eq. (6) was determined as a monotonically increasing function of the reciprocal of R:

$$\frac{\sigma_{av}}{\sigma_{st}} = A \times \alpha_y + B \times C^{e^{-E \times \log\left(\frac{F}{R}\right)}} \quad (5)$$

$$\frac{\sigma_{dv}}{\sigma_{st}} = a \times \left(\frac{1}{R}\right)^b + c \quad (6)$$

where σ_{st} is the static bending stress, R is the radius of the curve [m], and A, B, C, E, a, b, and c are undetermined constants and obtained by approximating the base data, where $0<C<1$. α_y is the excess centrifugal acceleration and expressed by

$$\alpha_y = \frac{1}{3.6^2} \times \frac{V^2}{g \times R} - \frac{C_t}{G_c} \quad (7)$$

where V is the running speed, g is the gravitational acceleration, C_t is the cant amount, and G_c is the gauge. The constant F is given by

$$F = \frac{G \times (r_1 + r_2)}{2000 \times (r_1 - r_2)}, \quad (8)$$

where G is the distance between the wheel and rail contact points [m], r_1 is the turning radius of the outer wheel at the transition point, and r_2 is the turning radius of the inner wheel at the transition point. G, G_c, and C_t are schematically defined in Fig. 1. The transition point is the point where the contact position between the wheel and the rail changes with the lateral displacement of the axel and the contact position of the outer wheel transitions from the tread to the flange. The turning radii r_1 and r_2 are determined by contact geometry analysis using the cross-sectional profiles of the wheel and the rail.

By applying the operating conditions to the Eqs. (5) and (6) obtained in this way, the stress spectrum in each element can be obtained. This stress spectrum is integrated over the evaluation segment to obtain the stress spectrum. The following two methods are used to determine the equivalent stress from the stress spectrum thus obtained:

(1) The stress and the stress frequency are summed over the entire line to be evaluated, the stress spectrum is calculated, and the equivalent stress is obtained.
(2) The equivalent stress is calculated from the stress spectrum for each evaluation segment. Finally, the equivalent stress for the entire evaluated line is obtained.

3. Fatigue Testing of Full-scale Railway Axles

3.1 Test axles and test methods

In this study, we conducted full-scale fatigue tests on two types of axles widely used in Japan: quenched and tempered axles SFA 640 for conventional railway vehicles and induction-hardened axles S38C-QA for high-speed railway vehicles. Both types of axles are made of steels with similar chemical compositions. For example, the chemical composition of the SFA640 steel is 0.39% C, 0.28% Si, 0.78% Mn, 0.0010% P, and 0.007% S. The axle material is first forged into a rough shape and then quenched and tempered. After this step, the quenched and tempered axle is machined to its final shape to become a product. On the other hand, the induction-hardened axle is roughly machined, induction hardened, and tempered at a low temperature, and then finish machined to its final shape to become a product. The quenched and tempered axles we tested had a tensile strength of over 640 MPa. The material of the quenched and tem-

Table 1 Size of the tested axles and features of the failures

Class	Evaluation part	Diameter of fitted part D [mm]	Diameter of axle body d [mm]	Diameter ratio D/d*	Detected failure for life evaluation
Quenched and tempered axle SFA640	Fitted part (Wheel seat)	191 192	194 195	0.98 (1.00)* 0.98 (1.00)*	MT flaw (Breakage**)
	Non-fitted part (Axle body)	191 200	166 166	1.15 1.20	Breakage
Induction hardened axle S38C-QA	Fitted part (Wheel seat)	209 209	207 190	1.01 1.10	Micro crack
	Non-fitted part (Axle body)	195	150	1.30	Breakage***

*D/d can be considered 1.00 for simplicity. **Additionally tested. ***Not broken in experiment.

pered axles and the base material of induction hardened axles had a fine ferrite-pearlite structure. The surface hardened layer of the induction hardened axle had a fine tempered martensite structure with high hardness. Furthermore, large compressive residual stress was generated in the surface layer of the induction hardened axle, including the surface hardened layer.

Axles have fitted parts that are subject to fretting damage. It is thus necessary to evaluate axles by dividing them into fitted parts and non-fitted parts. Our testing process involved the use of a resonance-type axle fatigue testing machine developed by SincoTech Test & Engineering GmbH. This machine is capable of applying a deformation mode similar to that of rotating bending to an axle with the fitted part (wheel seat) of one wheel press fitted onto a wheel jig.

Table 1 shows the dimensions of the test axles. **Figure 4** shows an example of the shape of a test axle. The test axles were determined to have reached the end of their service life when one of the conditions shown in the right column of Table 1 was detected. Magnetic particle testing (MT) found a flaw (called an MT flaw) in the fitted part of the quenched and tempered axle, as performed for inspection and repair on in-service tracks. The non-fitted part was fatigue tested until it failed. Note that the term "failure" includes not only a breakage, but also a macro crack. This is because the allowable stress is determined from the fatigue limit corresponding to the presence or absence of failures according to the design concept of the axles and the strength design method in JRIS D1201-1. A micro crack was detected in the fitted part of the induction hardened axel by observation with an optical microscope. No MT flaws occurred at the stress that can be applied in the fatigue test.

Damage assessment requires the slope of the S–N curve in particular. For the regression of the S–N curve, the least squares method was adopted to minimize the residual lifetime on a log-log graph according to the JSME S 002 standard of the Japan Society of Mechanical Engineers (JSME).[25] The S–N curve was obtained by approximating Eq. (1) based on the fatigue test results of full-scale axles. The stress amplitude σ in Eq. (1) is the nominal stress of the wheel seat in the evaluation of the fitted part and is the maximum stress on the fillet surface in the evaluation of the non-fitted part.

3.2 Quenched and tempered axles

A quenched and tempered axle was prepared to evaluate the fatigue strength of fitted and non-fitted parts. Table 1 shows the diameter D of the fitted part (wheel seat) and the diameter d of the non-fitted part (central parallel portion) as the diameters of the evaluation parts as well as the diameter ratio D/d. These decisions were made with the intention of causing damage to the evaluation parts.

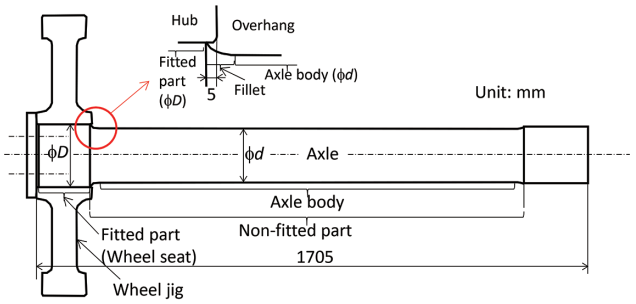

Fig. 4 Example of tested axle configuration[20]

The fatigue test of the fitted part was interrupted several times in mid-course. Each time, the axle was pulled out of the wheel jig by about 30 mm in the axial direction and magnetic particle tested. If no MT flaws were detected, the axle was pressed back into the wheel jig, and the test was resumed. This process was repeated until an MT flaw was detected. **Photo 1** shows the MT flaws found on the wheel seat after the fatigue test. The length of the MT flaws was about 2 mm. In addition, we used another axle and evaluated its life until the formation of a breakage or macro crack.

Figure 5 shows the S–N curves of the fitted part of a quenched and tempered axle. The S–N curve for breakage detection was directly approximated from the breakage data in the figure. The S–N curve for MT flaw detection was also approximated using the midpoint of the number of cycles between the two points before and after the detection of MT flaws (blue dashed line in the figure and noted as "m=6.8"). However, the slope of the approximated S–N curve for breakage detection was larger than that of the S–N curve for MT flaw detection. In other words, the exponent m of the S–N curve for breakage detection is the reciprocal of the slope and is smaller than that of the S–N curve for MT flaw detection. This result means that both S–N curves intersect in the long life region. Such behavior is physically difficult to imagine. Therefore, the exponent m obtained from the S–N curve for breakage detection was also applied to the approximation of the S–N curve for MT flaw detection, and the following equation was obtained.

$$N = 1.4 \times 10^{16} \cdot \sigma^{-5} \quad (9)$$

In the evaluation of the non-fitted part, the number of cycles to the formation of macro cracks with a length of 20 to 130 mm (corresponding to one-quarter of the circumference of the axle) was determined as the life to breakage. **Photo 2** shows a photograph of a macro crack on the outer surface of the axle after the fatigue test. The S–N diagram for the non-fitted part of the quenched and tem-

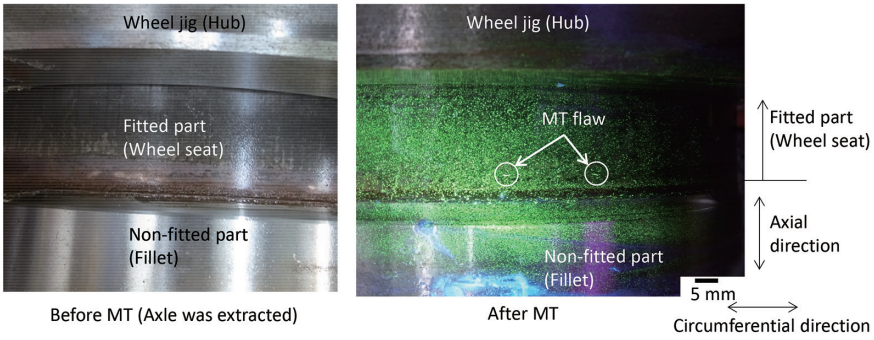

SFA640, σ = 100 MPa at wheel seat, N=1.5x10^6, MT flaw is approx. 2 mm in length.

Photo 1 Outer view of the wheel seat before/after MT and MT flaw of a quenched and tempered axle after fatigue test (Circles indicate MT flaws)[20)]

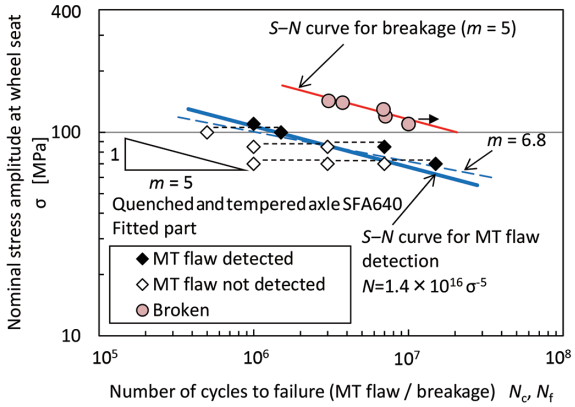

Fig. 5 *S–N* diagram for fitted part of the quenched and tempered axle[20)]

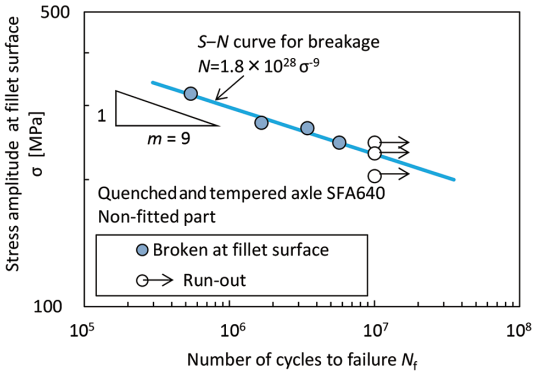

Fig. 6 *S–N* diagram for non-fitted part of the quenched and tempered axle[20)]

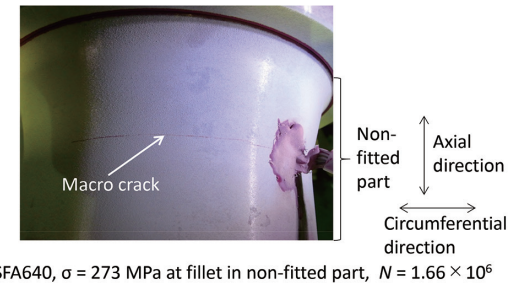

SFA640, σ = 273 MPa at fillet in non-fitted part, N = 1.66 × 10^6

Photo 2 Outer view of a macroscopic crack on the non-fitted part of the quenched and tempered axle after fatigue test[20)]

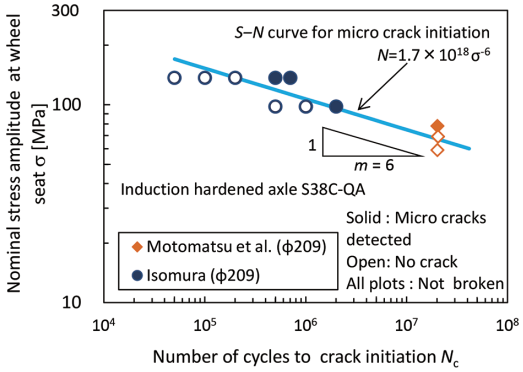

Fig. 7 *S–N* diagram for fitted part of the induction hardened axle (Some of the data were quoted from reference 26), 27))[20)]

pered axle shown in **Fig. 6** and the following equation were obtained.

$$N = 1.8 \times 10^{28} \cdot \sigma^{-9} \quad (10)$$

3.3 Induction hardened axle

The fatigue test of fitted parts was conducted using an induction hardened axle with the dimensions shown in Table 1.[26, 27)] This test provided the life to the occurrence of micro cracks. A microcrack is a crack with a length of 30 μm or more, as observed with an optical microscope. **Figure 7** shows the *S–N* diagram of the fitted part of the induction hardened axle constructed by using the above data. From this diagram, the *S–N* curve was approximated using the number of cycles at the midpoint of two points before and after the detection of a micro crack, and the following equation was obtained:

$$N = 1.7 \times 10^{18} \cdot \sigma^{-6} \quad (11)$$

The fatigue test of the non-fitted parts was conducted using an induction hardened axle with the dimensions shown in Table 1. However, when the axle was tested up to 1×10^7 cycles with a maximum stress of 380 MPa on the fillet surface, the axle was not damaged. Not even MT flaws were detected on this axle. Incidentally, under higher stress conditions, the temperature of the axle surface rose too high to continue the test. For this reason, we changed the test method to a repeated bending fatigue test using an electrohydraulic servo-type fatigue testing machine. We have the prospect of solving the problems mentioned above. We are now accumulating *S–N* data and proceeding with our study toward the revision of JRIS D1201.

4. Discussion

4.1 Exponents *m* of *S–N* curves specified in JRIS D1201-2

Table 2 summarizes the exponents *m* specified in JRIS D1201-

Table 2 Index of *S–N* curve

Class	Evaluation part	m^*
Quenched and tempered axle SFA640	Fitted part	5
	Non-fitted part**	9
Induction hardened axle S38C-QA	Fitted part	6
	Non-fitted part**	9***

*$N=A^*\sigma^{-m}$, N[cycle], σ[MPa]. **Surface roughness $Ra=3.2\,\mu$m.
***Determined as the same value as that of SFA640.

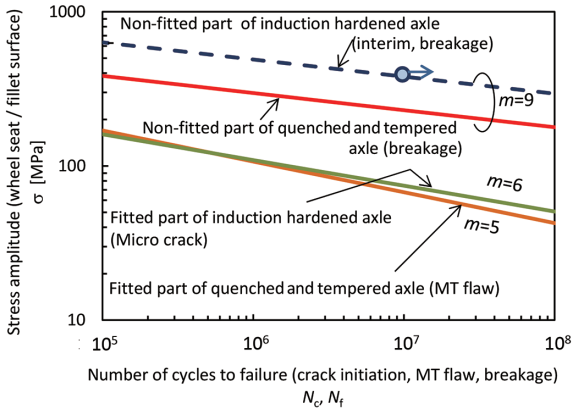

Fig. 8 Comparison of *S–N* curves between axle classes and evaluation parts[20]

2. These m values were obtained by organizing the fatigue test results described in the previous sections of this report or the results of fatigue tests conducted in the past. **Figure 8** comparatively shows the *S–N* curves for the respective axel types and the respective evaluation parts. Since no experimental data were available for the exponents m of the non-fitted parts of induction hardened axles, the exponents m were set to the same values as the exponents m of the non-fitted parts of quenched and tempered axles. In Table 2, the exponents m of the fitted parts are smaller than those of the non-fitted parts, regardless of the axle type. This result is probably obtained because the fitted parts have lower stress concentration and higher fatigue strength than the non-fitted parts. This tendency has been confirmed in other products. For example, according to the fatigue design criteria for welded joints and components[28] and the FKM Guideline,[17] the m value of welded components is smaller than that of smooth components. Beretta et al.[6] estimated the *S–N* curves of full-scale axles from the data of small axles. They obtained the *S–N* curve of full-scale axles by connecting the 10^4 cycle strength of small axles with the fatigue limit of the full-scale axles. Their result means that the exponent m increases and decreases with the fatigue limit. These tendencies qualitatively correspond to those shown in Fig. 8.

4.2 Advantages of relative evaluation by equivalent stress ratio

In the future, the m value may vary from the provisional values shown in Table 2 if the *S–N* curves of the non-fitted parts of the induction hardened axles are clarified. Furthermore, the m value may change slightly with the shape of the axle, i.e., the D/d value, and with the presence or absence of an overhang. However, the results of the evaluation using the equivalent stress ratio of the proposed damage assessment method may be relatively unaffected by the change in the m value. This consideration is verified using the stress spectra of two virtual trains, A and B, shown in **Fig. 9**. Train A is assumed to have a fully safe operating record, and train B is assumed to be the subject of fatigue damage evaluation. These stress spectra were generated so that the most frequent stress in trains A and B was 28 MPa and 22 MPa, respectively, that the highest stress was the same at 70 MPa, and that the total frequency was the same at 2.69 $\times10^5$. The equivalent stress was calculated for the m value range of 7 to 11 by substituting the stress value and stress frequency into Eq. (3) for all stress levels. The equivalent stress of train A was set as the reference value $\sigma_{eq,R}$ and the equivalent stress of train B was set as the design evaluation value $\sigma_{eq}{}^*$. Then, the equivalent stress ratio R_S was obtained by substituting $\sigma_{eq,R}$ and $\sigma_{eq}{}^*$ into Eq. (4). **Figure 10** shows the changes in the equivalent stress and equivalent stress ratio with respect to the m value. When the m value increased from 7 to 11, the equivalent stress of train B increased by 25%, but the equivalent stress ratio decreased by 8%. Therefore, when the m value changed, the change rate of the equivalent stress ratio was lower than that of the equivalent stress. This result suggests that the proposed evaluation method that uses the equivalent stress ratio is superior to the general evaluation method that directly uses the equivalent stress in terms of the stability of the evaluation results.

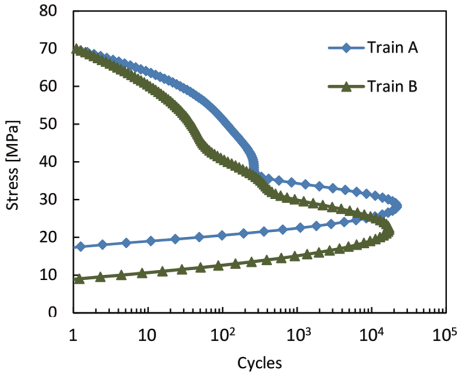

Fig. 9 Stress spectra with the different most frequent stresses of the two virtual trains[20]

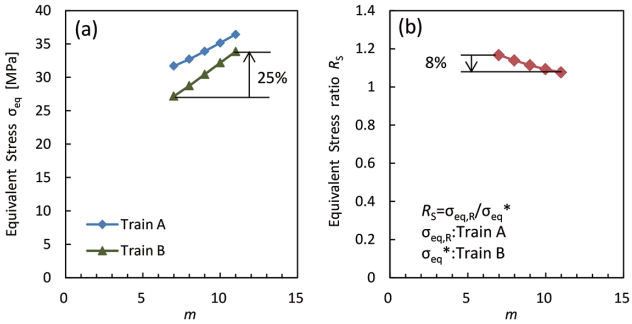

Fig. 10 Variations in the equivalent stresses and equivalent stress ratio with the index of *S–N* curve m[20]
(a) Equivalent stress (b) Equivalent stress ratio

4.3 Fatigue strength evaluation of fitted parts of induction hardened axles in high-stress and long-life regions

JRIS D1201-2 adopted the past literature data in the fatigue strength evaluation of the fitted parts of induction hardened axles. Although our data were not adopted in this evaluation, we manufactured induction hardened axles with $D=166$ mm, $d=160$ mm, and $D/d=1.04$ and fatigue tested them at high stresses. **Figure 11** shows the test results plotted in Fig. 7. As shown in Fig. 11, failures and

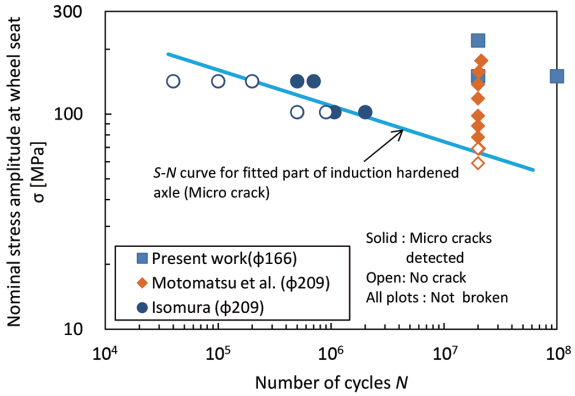

Fig. 11 ***S–N*** **plot for the fitted part of an induction-hardened axle and additional fatigue test results (Some of the data were quoted from reference 26), 27))[20)]**

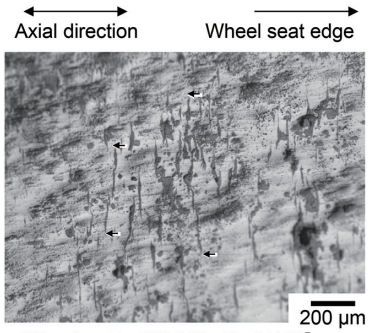

σ(Wheel seat) = 220 MPa, $N = 2 \times 10^7$

Photo 3 Microscopic cracks observed via an optical microscope on the fitted surface of an induction hardened axle (Arrows indicate crack tips)

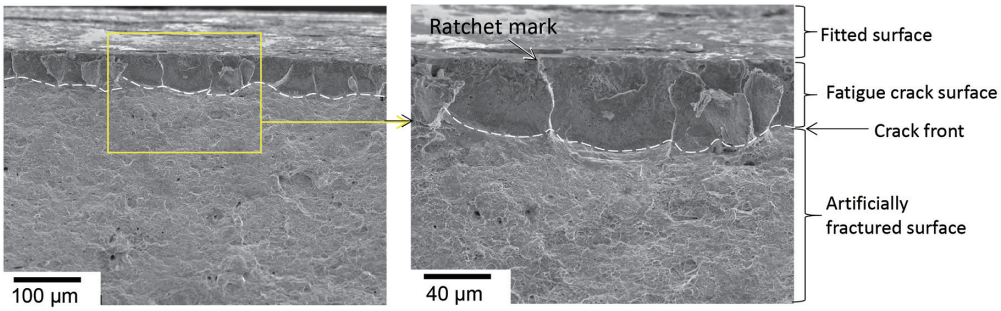

σ(Wheel seat) = 220 MPa, $N = 2 \times 10^7$

Photo 4 SEM images of crack surfaces with fretting fatigue cracks initiated on the fitted surface of an induction hardened axle

MT flaws were not detected when the fitted part was loaded with the nominal stress of 220 MPa for 2×10^7 cycles. After the test, the axle was removed from the wheel jig, and the surface of the fitted part of the axle was observed with an optical microscope. As shown in **Photo 3**, fretting damage was observed, that is, many fretting fatigue cracks involving fretting corrosion. A specimen containing fretting cracks was removed from the axle, cooled in liquid nitrogen, and artificially fractured to open the fatigue cracks. **Photo 4** shows SEM fractographs of the crack fracture surface. Many ratchet marks were observed on the fracture surface. This condition means that multiple fine cracks occurred, coalesced, and propagated. The longest crack was 0.53 mm long on the surface but was not detected by magnetic particle testing. Therefore, the fatigue limit for the occurrence of MT flaws is higher than 220 MPa and is more than three times the fatigue limit (70 MPa) for fine crack initiation of the same axle type. These characteristics may be ascribed to the suppression of crack propagation by the large compressive residual stress induced by induction hardening.

5. Conclusions

In this report, we outlined JRIS D1201-2: Rolling stock - Axle strength - Part 2: Fatigue damage evaluation method and described the fatigue properties of full-scale axles obtained in the process of formulating the standard. The damage evaluation method proposed in the standard is superior in terms of safety risk reduction as compared to the fatigue damage evaluation methods proposed in previous studies on railway axles because it involves a relative comparison with the equivalent stress of reference axles with safe operating records during safety evaluation. According to the fatigue test results of full-scale axles, the exponent m, which is the inverse of the slope of the S–N curve, was set to 5 for the fitted parts of quenched and tempered axles, 9 for the non-fitted parts of quenched and tempered axles, and 6 for the fitted parts of induction hardened axles. Since no experimental data were available for the non-fitted parts of induction hardened axles, the exponent m was provisionally set to 9 in the same way as that for quenched and tempered axles. This m value of 9 may be changed when new fatigue data are obtained.

In the future, we plan to clarify the S–N curves of the non-fitted parts of induction hardened axles and accumulate data on axle damage during operation by applying this evaluation method. We will then use the obtained results to improve the axle design method further.

Acknowledgments

The authors would like to express their gratitude to the members of the standard drafting committee and the standard review committee of JRIS D1201-1 and -2, especially Kazuhiko Tezuka (TESS Co., Ltd.), Hiromichi Ishizuka (formerly of the Railway Technical Research Institute), Kazunari Makino (Railway Technical Research Institute), and Masataka Yamamoto (Railway Technical Research Institute), for their helpful discussions in drafting and reviewing the two standards. The authors would also like to thank Machi Nakata (College of Industrial Technology, formerly of Nippon Steel & Sumitomo Metal Corporation) for his valuable advice in considering the concept of the standards.

References

1) JIS E 4501:1995: Railway rolling stock - Design methods for strength of axles
2) Tezuka, K., Tanaka, S.: 9th Int. Wheelset Congress, Montreal, 3–4–1-8, 1988
3) JRIS D1201-1:2016: Rolling stock - Axle strength - Part 1: Design method
4) JRIS D1201-2:2016: Rolling stock - Axle strength - Part 2: Fatigue damage evaluation method
5) Zerbst, U., Schödel, M., Beier, H.Th.: Engineering Fracture Mechanics. 78, 793 (2011)
6) Beretta, S., Regazzi, D.: International Journal of Fatigue. 86, 13 (2016)
7) Traupe, M., Jenne, S., Lütkepohl, K., Varfolomeev, I.: International Journal of Fatigue. 86, 44 (2016)
8) Regazzi, D., Beretta, S., Carboni, M.: Engineering Fracture Mechanics. 131, 587 (2014)
9) Gänser, H.P., Maierhofer, J., Tichy, R., Zivkovic, I., Pippan, R., Luke, M., Varfolomeev, I.: International Journal of Fatigue. 86, 52 (2016)
10) Cervello, S.: International Journal of Fatigue. 86, 2 (2016)
11) Sander, M., Richard, H.A.: Engineering Fracture Mechanics. 78, 754 (2011)
12) Luke, M., Varfolomeev, I., Lutkepohl, K., Esderts, A.: Engineering Failure Analysis. 17, 617 (2010)
13) Wu, S.C., Liu, Y.X., Li, C.H., Kang, G.Z., Liang, S.L.: Engineering Fracture Mechanics. 197, 176 (2018)
14) Wu, S.C., Zhang, S.Q., Xu, Z.W., Kang, G.Z., Cai, L.X.: International Journal of Fatigue. 93, 64 (2016)
15) Wu, S.C., Xu, Z.W., Kang, G.Z., He, W.F.: International Journal of Fatigue. 117, 90 (2018)
16) Xu, Z.W., Wu, S.C., Wang, X.S.: International Journal of Fatigue. 123, 79 (2019)
17) Rennert, R. et al.: FKM Guideline: Analytical strength assessment of components–Made of Steel, Cast Iron and Aluminum Materials in Mechanical Engineering, 6th revised edition, Frankfurt: FKM, 2012
18) Makino, T., Yamamoto, M., Hirakawa, K.: Journal of the Society of Materials Science, Japan. 46 (10), 1178 (1997)
19) Makino, T., Yamamoto, M., Hirakawa, K.: 12th International Wheelset Congress, Qingdao, 147 (1998)
20) Makino, T., Sakai, H., Kozuka, C., Yamazaki, Y., Yamamoto, M., Minoshima, K.: International Journal of Fatigue. 132, 105361 (2020)
21) Braghin, F., Bruni, S., Cervello, S., Chiudinelli, M.: 16th International Wheelset Congress, Cape Town, Session 1.2 (2010)
22) Watson. A.S., Timmis. K.: Engineering Fracture Mechanics. 78, 836 (2011)
23) Shabana, A.A., Zaazaa, K.E., Sugiyama, H.: Railroad Vehicle Dynamics–A Computational Approach. CRC press, 2007
24) Kaufmann, K.W.: Oecologia (Berl). 49, 293 (1981)
25) JSME S 002-1994: Standard Method of Statistical Fatigue Testing (Revised Edition)
26) Isomura, S.: JREA. 38 (12), 23563 (1995)
27) Motomatsu, H., Tezuka, K., Maebashi, E.: RTRI Report. 6 (3), 29 (1992)
28) The International Institute of Welding (IIW): Fatigue design of welded joints and components. Abington publishing, 1996, p.34-56

Taizo MAKINO
Dr. Eng., Leading Researcher
Steel Research Laboratories
1-8 Fuso-cho, Amagasaki City, Hyogo Pref. 660-0891

Hiroki SAKAI
Chief Manager, Head of Dept.
Railway Wheel & Axle Engineering Dept.
Railway Wheel, Axle & Bogie Div.
Kansai Works

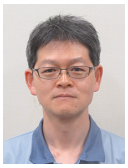

Chihiro KOZUKA
Senior Manager
Railway Wheel & Axle Quality Design Section
Railway Wheel, Axle & Bogie Quality Control Dept.
Quality Management Div.
Kansai Works

Yosuke YAMAZAKI
Dr. Eng., Senior Researcher
Research Section-II
Applied Mechanics Research Dept.
Materials Reliability Research Lab.
Steel Research Laboratories

Miyuki YAMAMOTO
Dr. Eng., Professor
Graduate School of Engineering
Osaka University

Kohji MINOSHIMA
Dr. Eng., Principal
National Institute of Technology, Anan College